An Improvement to the High-Spectral-Resolution CO_2-Slicing Cloud-Top Altitude Retrieval

ROBERT E. HOLZ, STEVE ACKERMAN, PAOLO ANTONELLI, FRED NAGLE, AND ROBERT O. KNUTESON

CIMSS–University of Wisconsin—Madison, Madison, Wisconsin

MATTHEW MCGILL, DENNIS L. HLAVKA, AND WILLIAM D. HART

Goddard Space Flight Center, Greenbelt, Maryland

(Manuscript received 15 April 2005, in final form 27 September 2005)

ABSTRACT

An improvement to high-spectral-resolution infrared cloud-top altitude retrievals is compared to existing retrieval methods and cloud lidar measurements. The new method, CO_2 sorting, determines optimal channel pairs to which the CO_2 slicing retrieval will be applied. The new retrieval is applied to aircraft Scanning High-Resolution Interferometer Sounder (S-HIS) measurements. The results are compared to existing passive retrieval methods and coincident Cloud Physics Lidar (CPL) measurements. It is demonstrated that when CO_2 sorting is used to select channel pairs for CO_2 slicing there is an improvement in the retrieved cloud heights when compared to the CPL for the optically thin clouds (total optical depths less than 1.0). For geometrically thick but tenuous clouds, the infrared retrieved cloud tops underestimated the cloud height, when compared to those of the CPL, by greater than 2.5 km. For these cases the cloud heights retrieved by the S-HIS correlated closely with the level at which the CPL-integrated cloud optical depth was approximately 1.0.

1. Introduction

Retrieving an accurate cloud-top altitude is critical for determining the impact of clouds on the earth's radiation balance (Ohring et al. 2005). A cloud-top altitude can be retrieved using an infrared-measured brightness temperature and knowledge of the atmospheric temperature profile. This method will underestimate the cloud height if the field of view (FOV) is partially cloud filled or contains optically thin clouds. The CO_2-slicing technique was developed to overcome this limitation (Chahine 1974; Menzel et al. 1983; Smith and Platt 1978; Smith et al. 1974; Wylie and Menzel 1989). Validation studies have demonstrated that narrowband CO_2-slicing cloud-top retrievals frequently differ by greater than 1.5 km when compared to lidar measurements (Hawkinson et al. 2005). This is significantly larger than the requirement of errors less than 0.5 km needed for the climate data record (Ohring et al. 2005). The recent availability of the Atmospheric Infrared Sounder (AIRS) (Aumann et al. 2003) and the scheduled launch of the Hyperspectral Environmental Suite (HES) on the Geostationary Operational Environmental Satellite (GOES)-R will provide geostationary hyperspectral infrared measurements and the opportunity to improve the global cloud-top climatology.

The decreased spectral width of the high-spectral-resolution CO_2 channels and the orders of magnitude increase in the number of channels in the CO_2 band offers the possibility to decrease the error in the cloud-top retrievals. The CO_2 slicing technique applied to aircraft-based high-spectral-resolution measurements demonstrated this improved capability (Smith and Frey 1990). This investigation found that optimal CO_2-slicing channel pairs are a function of the cloud-top altitude and in order to optimize high-spectral-resolution CO_2 slicing a method to dynamically select the channel pairs was needed (Smith and Frey 1990).

This paper presents a new algorithm, CO_2 sorting, that addresses the channel pair selection by dynamically selecting the optimal CO_2-slicing channels pairs. This optimization to the hyperspectral CO_2-slicing-height retrieval is applied to aircraft high-spectral-resolution measurements in section 4 where it is com-

Corresponding author address: Dr. Robert E. Holz, 1225 W. Dayton, SSEC, Madison, WI 53706.
E-mail: reholz@ssec.wisc.edu

pared to fixed-channel pair CO_2-slicing (Smith and Frey 1990) and minimum local emissivity variance (MLEV) (Huang et al. 2004) high-spectral-resolution cloud-top retrievals. Coincident cloud lidar and imager measurements are used to evaluate the cloud-top retrieval sensitivity to cloud height, partially cloud filled FOV, and cloud optical depth in section 4 and 5.

2. Instrumentation

The Scanning High-Resolution Interferometer Sounder (S-HIS) was chosen for this investigation to develop and validate the high-spectral-resolution cloud-height retrievals. These well-calibrated aircraft-based high-spectral-resolution measurements where flown on the National Aeronautics and Space Administration (NASA) Earth Resources (ER)-2 at an altitude of approximately 20 km and provide the framework to develop new approaches to retrieving cloud-top altitude. The Cloud Physics Lidar (CPL) and Moderate Resolution Imaging Spectroradiometer (MODIS) Airborne Simulator (MAS) imager were flown along with the S-HIS on NASA's ER-2 and allow for an in-depth investigation of the cloud-height retrieval's sensitivity to cloud height, optical depth, and fractional cloud FOV. An overview of the instrumentation used in the analysis is presented in this section.

a. Scanning High-Resolution Interferometer Sounder

The S-HIS is an aircraft-based scanning Fourier transform interferometer designed to accurately measure atmospheric infrared radiances at high spectral and spatial resolutions (Revercomb et al. 1998). The S-HIS measures infrared radiances between 400 and 3000 cm^{-1} (3.0–25 μm), with a spectral resolution of approximately 0.5 cm^{-1}. The radiometric calibration allows for root-mean-square (rms) noise errors of less than 0.2 K at 260 K across the spectral bands, except near the band edges (Revercomb et al. 1998). The S-HIS has a 100-mrad field of view and is capable of cross-track scanning. In this paper only nadir fields of view are used in the analysis so that comparisons with nadir-viewing lidar can be performed. With a flight altitude of 20 km the nadir S-HIS field of view has approximately a 2-km-diameter surface footprint. The footprint is slightly oval along the flight track because of the 1-s dwell time and 200 m s^{-1} along-track velocity.

b. Cloud Physics Lidar

The CPL is a depolarization-sensitive cloud lidar developed by scientists at NASA Goddard Space Flight Center that flies on the ER-2 high-altitude aircraft (McGill et al. 2002). The CPL is an active remote sensing system that provides high-vertical-resolution cloud-height determinations (30 m) and retrieves cloud optical depth. The depolarization measurement allows for discrimination between ice and water. Photons backscattered on the surface of spherical water droplets have very little depolarization in contrast to high depolarization for ice crystals. The CPL laser transmits at 355, 532, and 1064 nm at a rate of 5000 shots per second. For this paper the 532-nm-channel data averaged to 1 s are used for comparison with the passive instruments. The high sample rate of the CPL results in a surface footprint that can be approximated as a continuous line with a diameter of 2 m. A robust collocation algorithm is used to collocate the CPL measurements with the S-HIS. On average, 10 CPL measurements are collocated with each 2-km S-HIS FOV. The collocated CPL measurements of cloud height, depolarization, and optical thickness are used to analyze the sensitivity of S-HIS cloud-top retrievals.

c. MODIS Airborne Simulator

The MAS (King et al. 1996) is a scanning spectrometer with a 2.5-mrad field of view. The MAS scene mirror scans at 7.25 Hz with a swath width of 42.96° from nadir, resulting in a 50-m nadir surface resolution with a swath width of 37.2 km when flown on the ER-2 20 km into the atmosphere (King et al. 1996). The MAS has 50 spectral channels located within the 0.55–14.2-μm spectral region. For this investigation the MAS high spatial resolution is utilized to determine cloud fractional coverage in individual S-HIS FOV. To identify the MAS pixels within the S-HIS footprint, the MAS is collocated with the S-HIS using a collocation algorithm presented in section 3e. The results of the collocation are applied to the MAS cloud mask, and the cloud fraction of the S-HIS FOV is determined (Ackerman et al. 1998). In this analysis if the MAS cloud mask determines the pixel to be cloudy or probably cloudy, the pixel is designated cloudy. All other classifications are considered clear.

3. Analysis methods

a. Fixed-channel CO_2 slicing

The CO_2-slicing algorithm has been used to retrieve cloud-top pressure using satellite measurements for over three decades (Menzel et al. 1983; Smith 1970; Smith and Platt 1978). The method relies on the strong temperature sensitivity of the 15-μm CO_2 absorption band and the well-mixed nature of carbon dioxide. The CO_2-slicing equation is as follows:

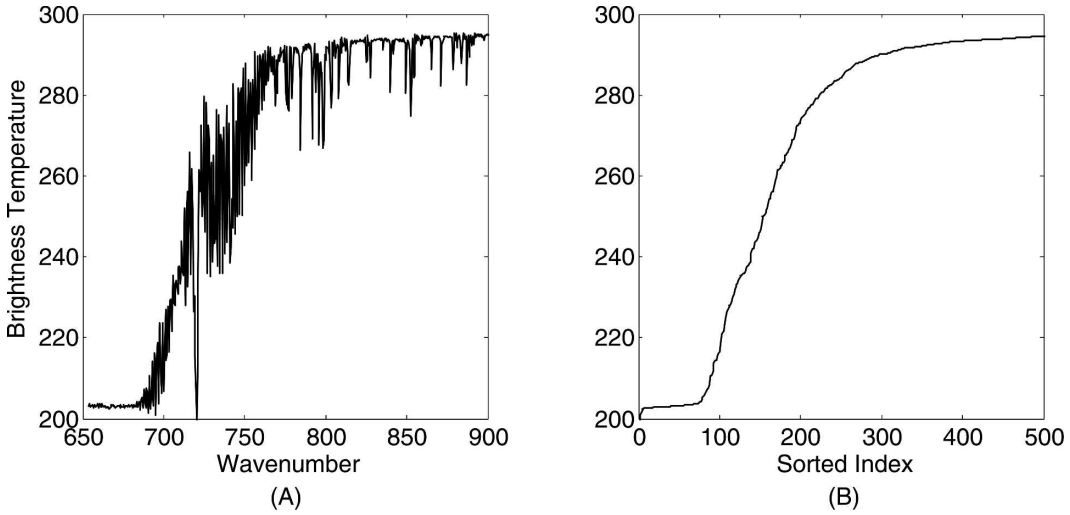

FIG. 1. (a) The S-HIS brightness temperature spectrum for the CO_2 absorption band. (b) The brightness temperatures sorted from the coldest to warmest channels are presented.

$$\frac{I(\upsilon_1) - I_{\mathrm{cl}}(\upsilon_1)}{I(\upsilon_2) - I_{\mathrm{cl}}(\upsilon_2)} = \frac{N\varepsilon(\upsilon_1)\displaystyle\int_{p_s}^{p_c} \tau(\upsilon_1,p)\frac{dB[\upsilon_1,T(p)]}{dp}\,dp}{N\varepsilon(\upsilon_2)\displaystyle\int_{p_s}^{p_c} \tau(\upsilon_2,p)\frac{dB[\upsilon_2,T(p)]}{dp}\,dp}, \tag{1}$$

where I is the measured radiance at the spectral region υ_1, and the subscripts reference the two channels selected for the retrieval; I_{cl} is the clear-sky radiance measured at the satellite; $\varepsilon(\upsilon)$ is the cloud emissivity at the channel frequency; N is the cloud fraction; p_c is the cloud pressure; p_s is the surface pressure; $\tau(\upsilon_1, p)$ is the spectral transmittance between the pressure levels p to the instrument; and $B[\upsilon, T(p)]$ is the Plank radiance for the selected channel frequency at pressure level p, where $T(p)$ is atmospheric temperature at pressure level p. In the current application, both $I_{\mathrm{cl}}(\upsilon)$ and $\tau(\upsilon, p)$ are computed using a line-by-line clear-sky radiative transfer model (LBLRTM) (Clough et al. 1981). The temperature and moisture profiles used for the simulations are retrieved using clear-sky S-HIS measurements.

The CO_2-slicing retrieval assumes the cloud effective emissivity ($N\varepsilon$) difference between spectrally close channels is negligible. With this assumption Eq. (1) becomes independent of the cloud effective emissivity. The cloud height is then determined by selecting the cloud pressure that minimizes the difference between the right and left side of Eq. (1).

In this investigation the fixed-channel pair hyperspectral CO_2-slicing algorithm is implemented using the method described (Smith and Frey 1990) using a subset of channels in the CO_2 band (700–800 cm^{-1}). The CO_2-slicing algorithm described in Eq. (1) is applied to each channel pair. If a unique cloud height is found the cloud effective emissivity ($N\varepsilon$) is calculated using Eq. (2),

$$N\varepsilon_{\upsilon} = \frac{I(\upsilon) - I_{\mathrm{cl}}(\upsilon)}{I_{\mathrm{cb}}(\upsilon,p_c) - I_{\mathrm{cl}}(\upsilon)}. \tag{2}$$

If the cloud emissivity is greater than 0.1 and less than 1.0, the channel pair solution is accepted. A difference function is then computed for all valid channel pair solutions as described by

$$\Gamma = \sum_{\upsilon_{\mathrm{start}}}^{\upsilon_{\mathrm{end}}} \{I(\upsilon) - I_{\mathrm{cl}}(\upsilon) - N\varepsilon[I_{\mathrm{cb}}(\upsilon,p_c) - I_{\mathrm{cl}}(\upsilon)]\}, \tag{3}$$

where $I(\upsilon)$ is the measured S-HIS radiance in channel υ, $I_{\mathrm{cl}}(\upsilon)$ is the calculated clear-sky radiance, and $I_{\mathrm{cb}}(\upsilon,p)$ is

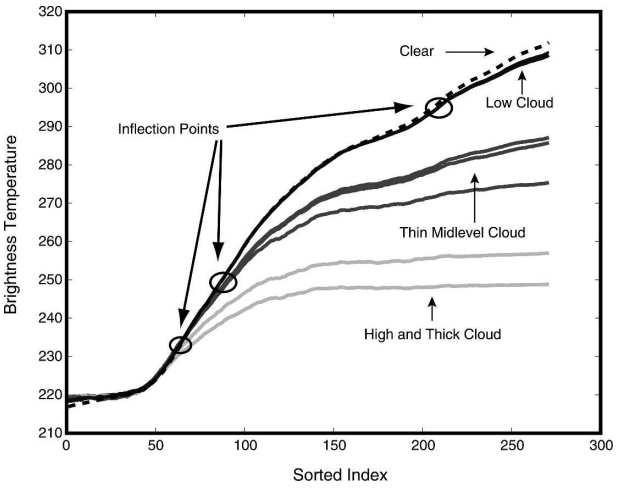

FIG. 2. The clear-sky-sorted index applied to low, high, and optically thin S-HIS cloudy FOVs. The dashed curve is the sorted clear-sky FOV. The inflection points are circled in the figure.

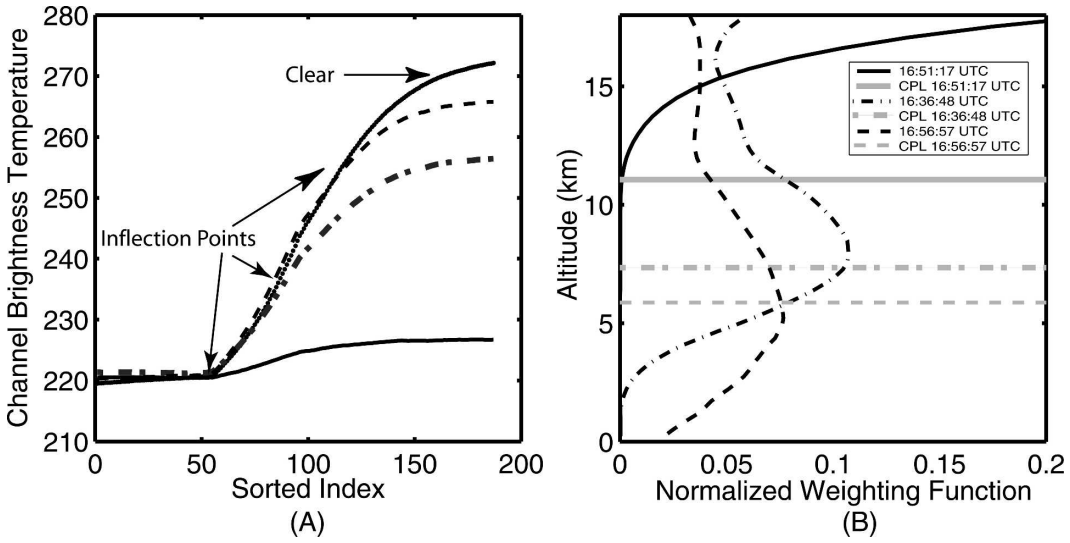

FIG. 3. Cloudy-sorted BT spectrums are presented with the clear-sky-sorted BT. The weighting functions of the channel picked to be the inflection point in (b) are presented in (a). The cloud height determined using the collocated CPL measurement (horizontal lines) is included in the figure on the right.

the calculated opaque cloud radiance at the cloud pressure level p_c retrieved using CO_2 slicing. Respectively, V_{start} and V_{end} represent the first and last channels used as pairs in the retrieval. The height resulting from the channel pair that minimizes Eq. (3) is considered the optimal cloud height.

The decrease in the spectral width of high-spectral-resolution infrared measurements results in narrower weighting functions, offering the potential for improved vertical resolution (Smith and Frey 1990). However, the large increase in the number of channel pairs introduces the added complexity of selecting optimal CO_2-slicing channel pairs (Smith and Frey 1990). The optimal pairs are dependent on the cloud height (Smith and Frey 1990). If opaque channels are selected the channel weighting function will peak well above the cloud height and the measured radiance will include little cloud emission. For these channels the CO_2-slicing retrieval will have limited skill. The optimal channels are ones that have a significant cloud signal while reducing the sensitivity to the lower-atmospheric emission that dominates the uncertainties in the clear-sky calculation. A channel with a weighting function that peaks near the cloud-top altitude will contain a significant cloud signal while reducing the sensitivity to the lower atmosphere. A reliable method of selecting these channels is needed to maximize the accuracy of the CO_2-slicing retrieval.

b. CO_2 sorting

The paper presents the CO_2-sorting method designed to select the optimal channel pairs for CO_2 slicing. Hyperspectral infrared measurements are capable of resolving spectral features in the 15-μm CO_2 band (680–770 cm^{-1}), as presented in Fig. 1. For these channels there is a trend to warmer brightness temperatures with increasing wavenumber because of the decrease in the opacity of the channels. However, the spectral structure of the CO_2 band results in significant fluctuation in the opacity of the channels. Assuming an atmosphere that decreases in temperature with height, the measured brightness temperatures are proportional to the transparency of the channel. Using this relationship, if the channels are sorted relative to a clear-sky brightness temperature they are also sorted relative to their opac-

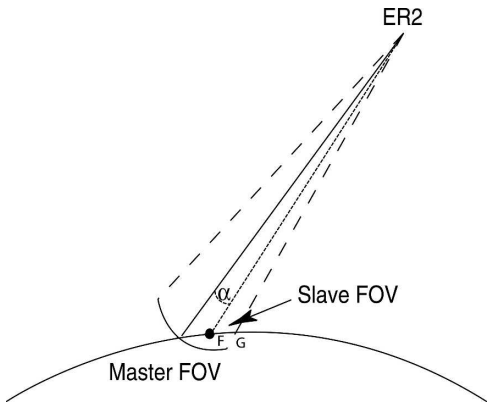

FIG. 4. The collocation algorithm geometry is illustrated. The master field of view is defined as the half-angular field of view of the master instrument (S-HIS). The angle between the slave instrument (MAS or S-HIS) geolocation (F) and the center axis of the master field is designated α in this figure. If α is less than the half-angular field of view of the master instrument, the slave pixel is considered to be within the field of view of the S-HIS.

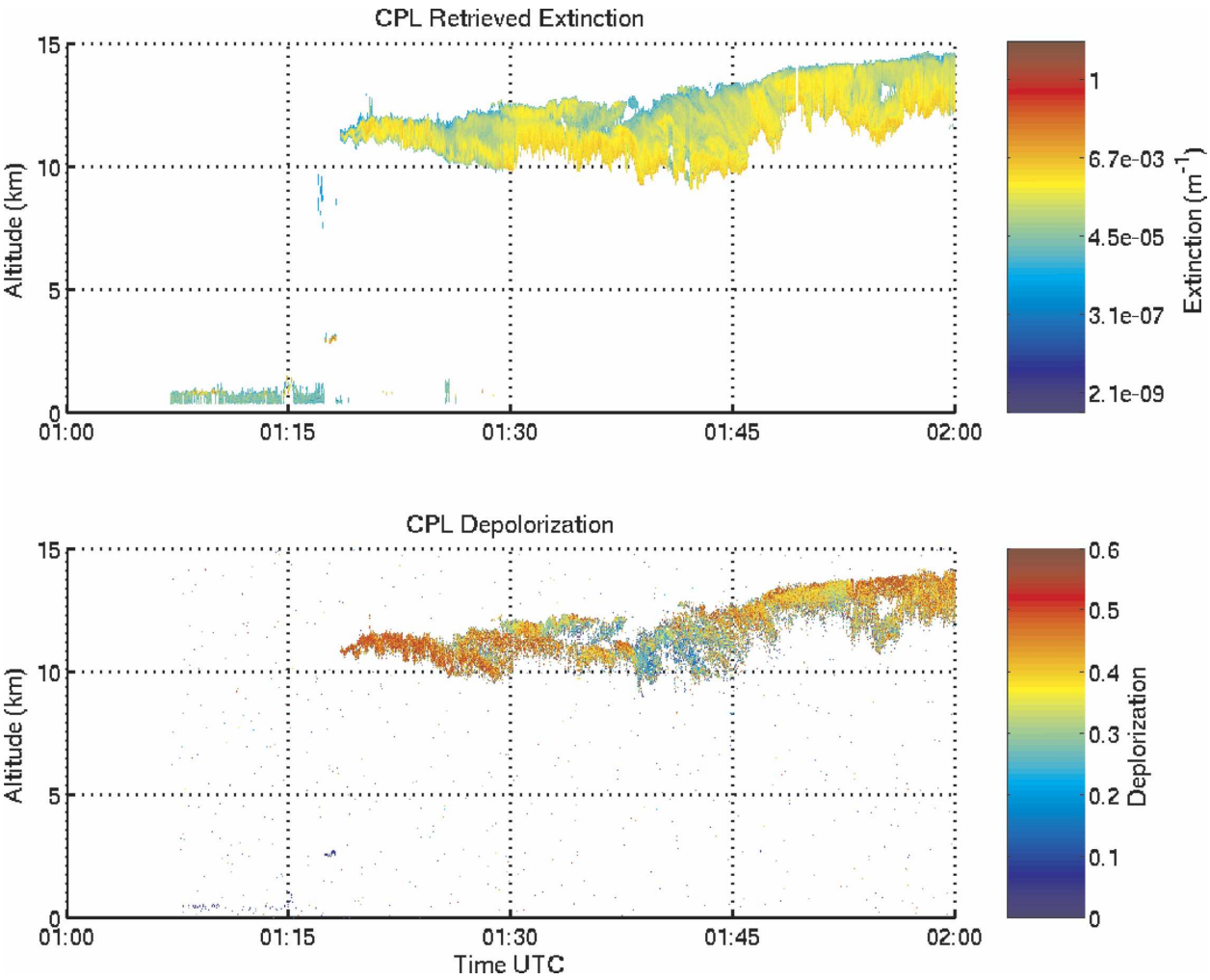

FIG. 5. The CPL-retrieved extinction and depolarization cross sections for the 22 February THORPEX flight.

ity. This approach is similar to McNally's cloud detection algorithm (McNally and Watts 2003); however, in CO_2 sorting the sorting is based on the measured cloud brightness temperature, not the peak of the computed channel, eliminating the clear-sky transmittance calculation. Sorted clear-sky brightness temperatures are presented in Fig. 1. The sorting results in a smoothly increasing function of brightness temperature, starting with the coldest, most opaque channel to the warmest and most transparent channels in the CO_2 band. The sorting orders the channels by the atmospheric level at which the channels' weighting function peaks.

The clear-sky-sorted channel indices are used to reorder the brightness temperature spectra for cloudy FOVs. Channels that have weighting functions peaking above the cloud level will have negligible cloud emission. When clear and cloudy FOVs are compared, these channels will have little brightness temperature variation. Channels that have weighting functions that peak near or below the cloud level will contain significant cloud emission, resulting in brightness temperature differences between the clear and cloudy FOVs. The CO_2 sorting method applies the clear-sky-sorted index to a cloudy FOV and compares the reordered cloudy FOV to the sorted clear-sky brightness temperature. Examples of the clear-sky indices applied to cloudy FOVs are presented in Fig. 2. In this figure the most opaque channel whose radiance includes significant cloud emission occurs where the clear- and cloudy-sorted spectra deviate. This inflection point is illustrated in Fig. 2 for varying cloud altitudes and optical depths. The location of the inflection point is a function of the cloud altitude and cloud emissivity. For optically thick and high clouds the channels near the inflection point will have weighting functions that peak above the cloud altitude. Lower or optically thin clouds have inflection points

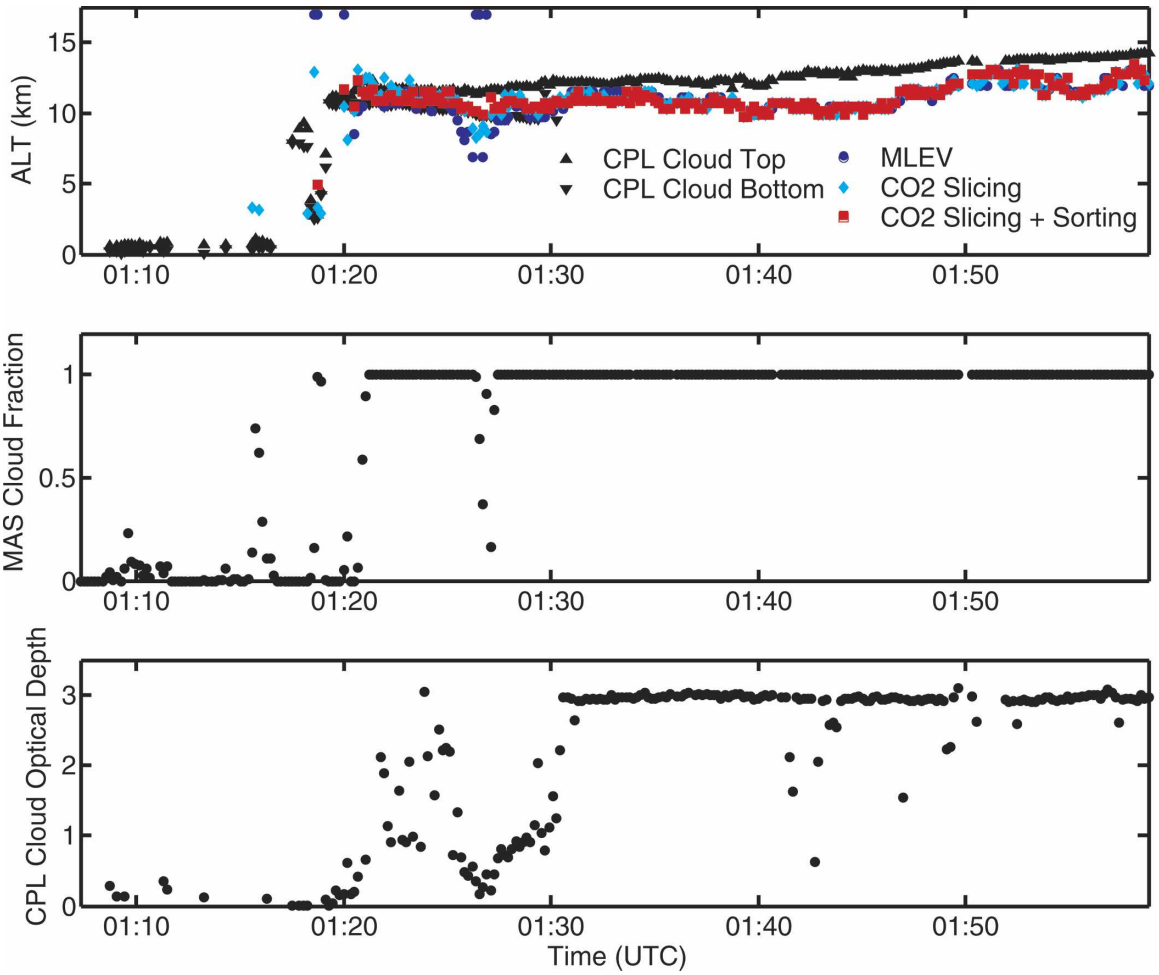

FIG. 6. (top) The S-HIS cloud-top retrievals collocated with the CPL-measured cloud-top and -base measurements from 22 Feb 2003. (middle) The S-HIS cloud fraction is computed using the collocated MAS cloud mask. (bottom) The mean CPL-measured optical depth is presented. The cloud top, base, and optical depth are the mean of all the CPL measurements found to be in each S-HIS field of view.

that have weighing functions peaking near the cloud altitude. The weighting functions of the channels selected by CO_2 sorting in Fig. 3a are presented in Fig. 3b.

The slope of the sorted cloudy scene is related to the cloud effective emissivity. For optically thick clouds the sorted brightness temperature asymptotes to the brightness temperature of the cloud. For optically thin clouds there is significant atmospheric emission from below the cloud and the sorted spectrum will not converge to a constant brightness temperature, as presented in Fig. 2.

c. *The hybrid CO_2 sorting–slicing cloud-height algorithm*

The inflection point found by CO_2 sorting represents the first channels with significant sensitivity to the cloud. Channels after the inflection point on the sorted spectrum will be sensitive to the cloud emission. The hybrid CO_2 sorting–slicing retrieval selects these channels as pairs to use for CO_2 slicing. To reduce cloud-height errors resulting from uncertainties in the surface temperature, emissivity, and lower-tropospheric water vapor and temperature profile, CO_2 sorting selects channels located between the inflection point and the first channel on the sorted spectrum determined to have significant surface emission. For a clear-sky FOV the sorted spectrum will converge to the surface brightness temperature as the channel's gaseous optical depth becomes small so that the signal measured in the channel is dominated by surface emission. The CO_2-sorting algorithm uses this decrease in slope to determine if the channel has significant surface emission. To further optimize the channel selection it was found that channels

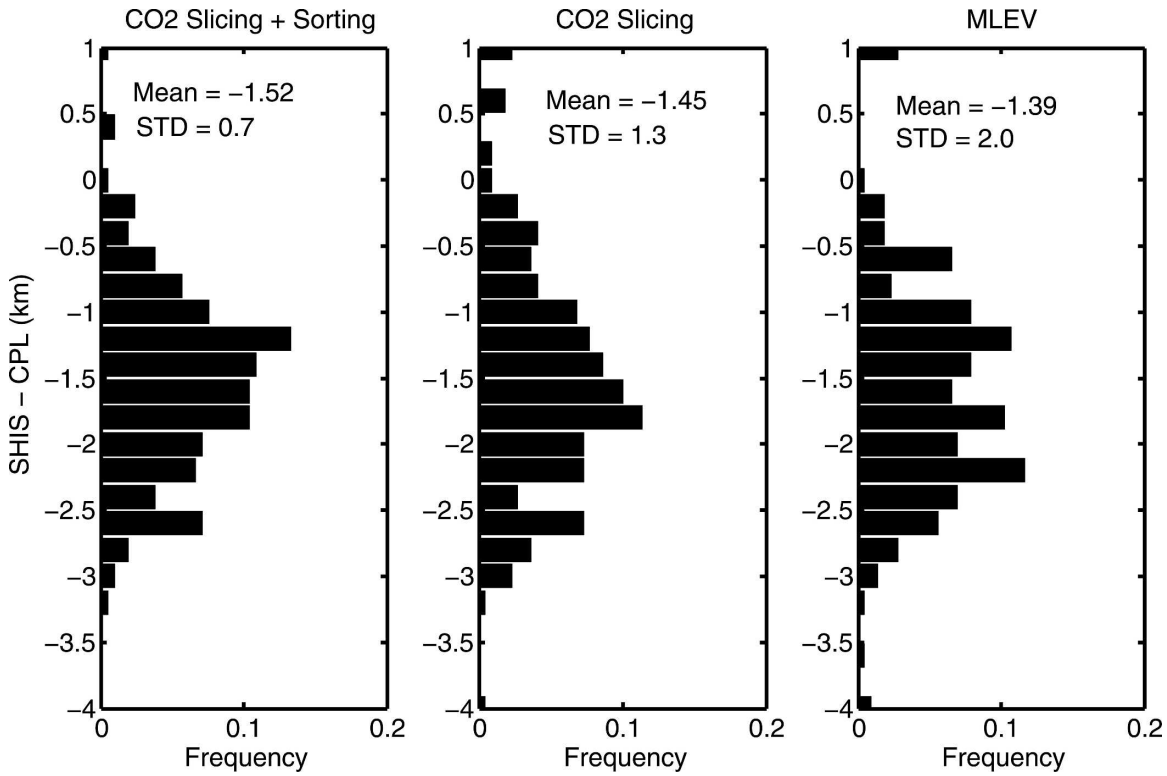

FIG. 7. The frequency of occurrence of the differences between the S-HIS cloud-top retrieval height compared to the mean of the collocated CPL cloud height for the different S-HIS retrievals for the 22 Feb 2003 flight between 1307 and 1358 UTC.

in the valleys of the CO_2 absorption region (650–800 cm^{-1}) produced the most consistent cloud-height results. For this reason only the channels selected by CO_2 sorting that are located in the valleys in the CO_2 absorption region are applied to CO_2 slicing.

d. MLEV

MLEV is a cloud-top retrieval algorithm designed to take advantage of hyperspectral measurements (Huang et al. 2004). MLEV uses the spectral channels between 750 and 950 cm^{-1} that include CO_2 and water vapor absorption lines (Huang et al. 2004). The ability of the hyperspectral infrared measurements to resolve the line structure allows for the calculation of cloud emissivity across absorption features. In contrast to the atmosphere, clouds have very little spectral structure across these wavelengths. The calculation of the cloud effective emissivity requires that the cloud altitude be known in order to calculate I_{cb} in the denominator of Eq. (2). An incorrect cloud height will result in channel-dependent variability in the cloud emissivity calculation. In MLEV the cloud emissivity is calculated for a cloud at each height in the atmospheric profile. The cloud height that minimizes the cloud emissivity spectral variability is chosen as the cloud-top height. The equations used to solve for MLEV are illustrated in Eqs. (4) and (5);

$$\mathrm{LEV}(p_c) = \sum_{\upsilon_{\mathrm{start}}}^{\upsilon_{\mathrm{end}}} [N\varepsilon(\upsilon,p_c) - \overline{N\varepsilon(p_c)}]^2, \tag{4}$$

where

$$\overline{N\varepsilon(p_c)} = \frac{\sum_{\upsilon_{\mathrm{start}}}^{\upsilon_{\mathrm{end}}} [N\varepsilon(\upsilon,p_c)]}{\Delta\upsilon}. \tag{5}$$

In these equations N is the cloud fraction, ε is the cloud emissivity, υ is the frequency of the channel, $\Delta\upsilon$ is the difference in frequency between $\upsilon_{\mathrm{start}}$ and υ_{end}, and p is the cloud pressure level. The cloud fractional emissivity is calculated for the channels between 750 and 950 cm^{-1} at each pressure level p_c. The pressure level (p_c) that minimizes the spectral variation (LEV) in this channel interval is considered the cloud pressure level. The number of pressure levels is defined by the atmospheric profile used in the calculation. The implementation of MLEV requires calculations of the cloudy radiances at each pressure level given in the temperature

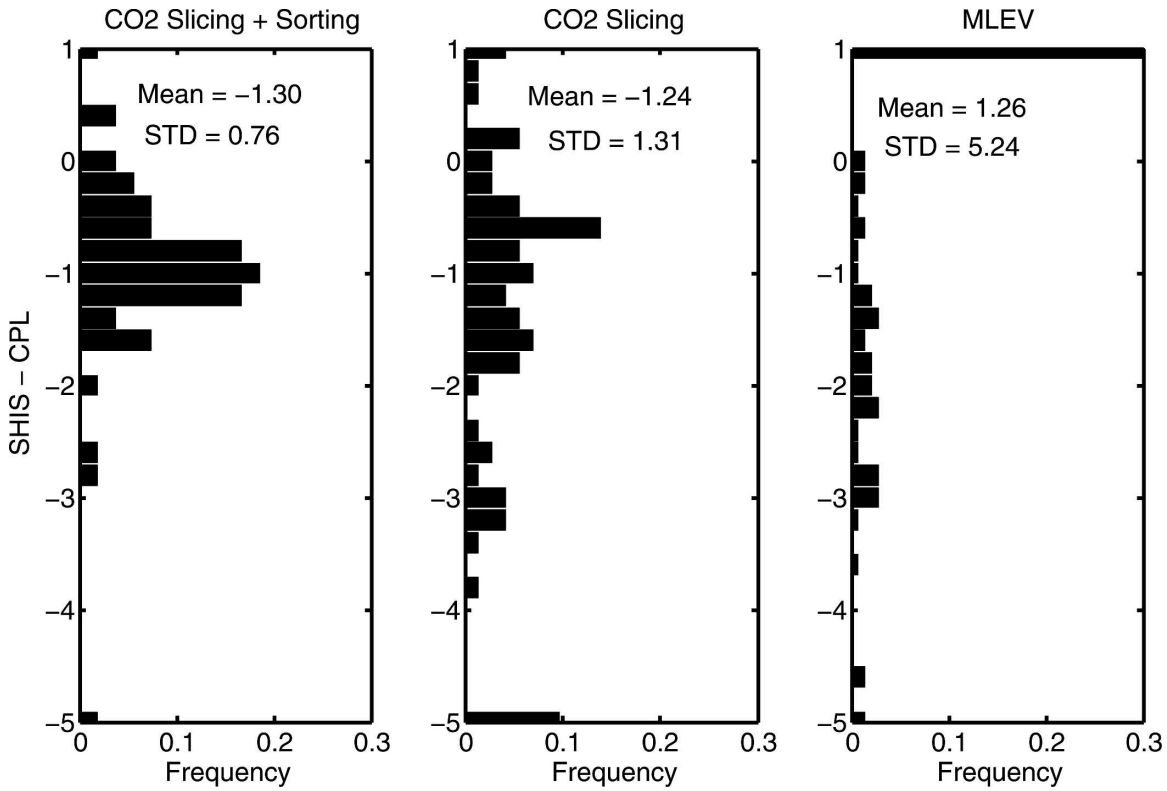

FIG. 8. The frequency of occurrence of the differences between the S-HIS cloud-top retrieval height compared to the mean of the collocated CPL cloud height for S-HIS FOV with CPL-measured cloud optical thickness less than 1.0 for the S-HIS retrievals from the 22 Feb 2003 flight.

and moisture profile. LBLRTM was used for our calculations using the S-HIS temperature and water vapor retrievals and dropsondes for water vapor and temperature profiles.

e. Collocation of imager and sounder data

In this paper S-HIS cloud-top retrievals are compared to CPL and MAS measurements. Quantitative comparisons of instruments with varying FOV and scan angles requires that the collocation of the instruments have errors less than the variability of the cloud structure in the FOV. For this investigation, a collocation algorithm originally developed for satellite collocation is adapted to work with the ER-2 instruments (Nagel 1998). The collocation designates the instrument with the larger FOV as the master instrument, in this case the S-HIS. The collocation locates all FOV of the secondary or "slave" instrument (MAS and CPL) that fall within each master FOV.

For this application the instruments are located on the same platform (ER-2), simplifying the inverse navigation. The master footprint on the earth's surface is difficult to describe mathematically (Nagel 1998). The collocation uses a simplification described in Fig. 4. The collocation finds all slave geolocated FOVs whose angle α, measured between the slave geolocation and the center of the geolocated master FOV, is less than the half-angular width of the master instrument.

The geolocation for slave and master instruments is computed using the same algorithm to reduce errors caused by algorithm differences used in the processed data for each instrument. For this reason, the collocation requires the aircraft position, role, heading, altitude, pitch, and instrument scan angle for both instruments. The instrument time is used to narrow the search region for finding collocated slave FOV, but is not used in the actual collocation. Because the collocation requires only the aircraft navigation information and master instrument FOV, it is easily adaptable to multiple instruments, in this case collocating both MAS and CPL with S-HIS.

To validate the collocation, MAS 11-μm brightness temperatures were compared to the S-HIS brightness temperatures. This comparison required convolving the spectral response function of the MAS 11-μm channel with the S-HIS measurements to produce S-HIS measurements at the MAS spectral resolution. For each S-HIS FOV the collocated MAS pixels are averaged to

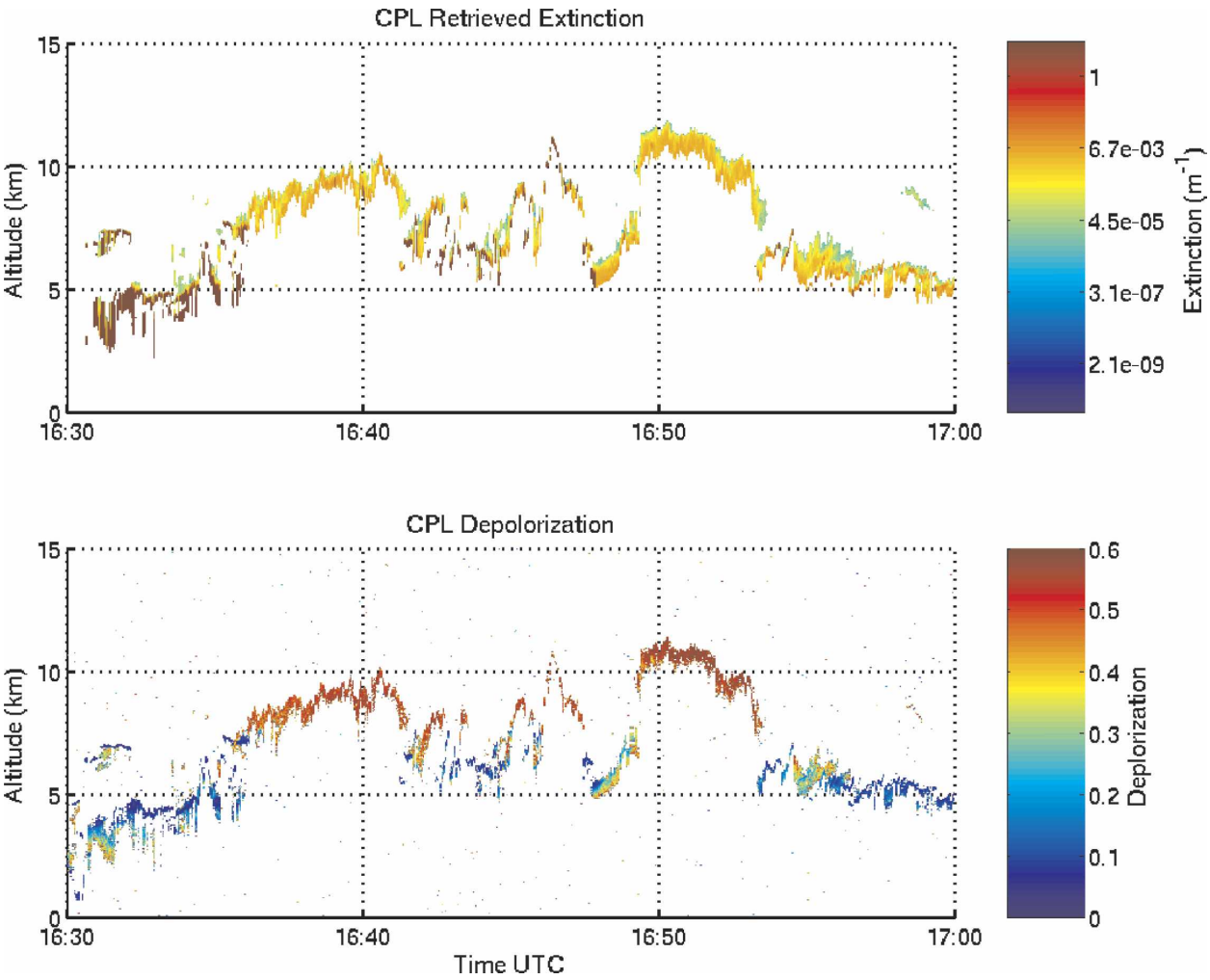

FIG. 9. The CPL-retrieved extinction and depolarization from the Atlantic ATReC experiment on 5 Dec 2003.

reduce the MAS spatial resolution to that of the S-HIS. The reduced-spectral-resolution S-HIS brightness temperature with the reduced-spatial-resolution MAS brightness temperature should be well correlated with an accurate collocation. Large deviations between averaged MAS and S-HIS measured brightness temperatures would result from errors in the collocation. This analysis was applied to the two flights with highly varying cloud scenes and resulted in correlations of 0.97 and 0.99. The slightly lower correlation for the first flight likely results from ER-2 navigation data problems during this flight. The high level of correlation between the S-HIS and MAS brightness temperature demonstrates the accuracy of the collocation.

4. Cloud-height retrieval validation

The hyperspectral cloud-top retrieval algorithms are applied to S-HIS measurements during The Observing System Research and Predictability Experiment (THORPEX), an experiment based in Hawaii (Shapiro and Thorpe 2002), and the Atlantic THORPEX Regional Campaign (ATReC) field campaign (Shapiro and Thorpe 2002) based in Bangor, Maine. For both missions the S-HIS flew with the CPL and MAS on the NASA ER-2 aircraft. These field campaigns were selected for their diverse clouds and atmospheric environments. In the following analysis the hyperspectral cloud-top retrieval algorithms are applied to selected flight segments. The results are compared to collocated CPL and MAS measurements.

a. THORPEX Pacific

ER-2 FLIGHT TRACK: 0107–0200 UTC

As part of the THORPEX field program on 22 February 2003, the ER-2 flew over the Pacific Ocean east of Hawaii. During the flight high cirrus clouds with tops at

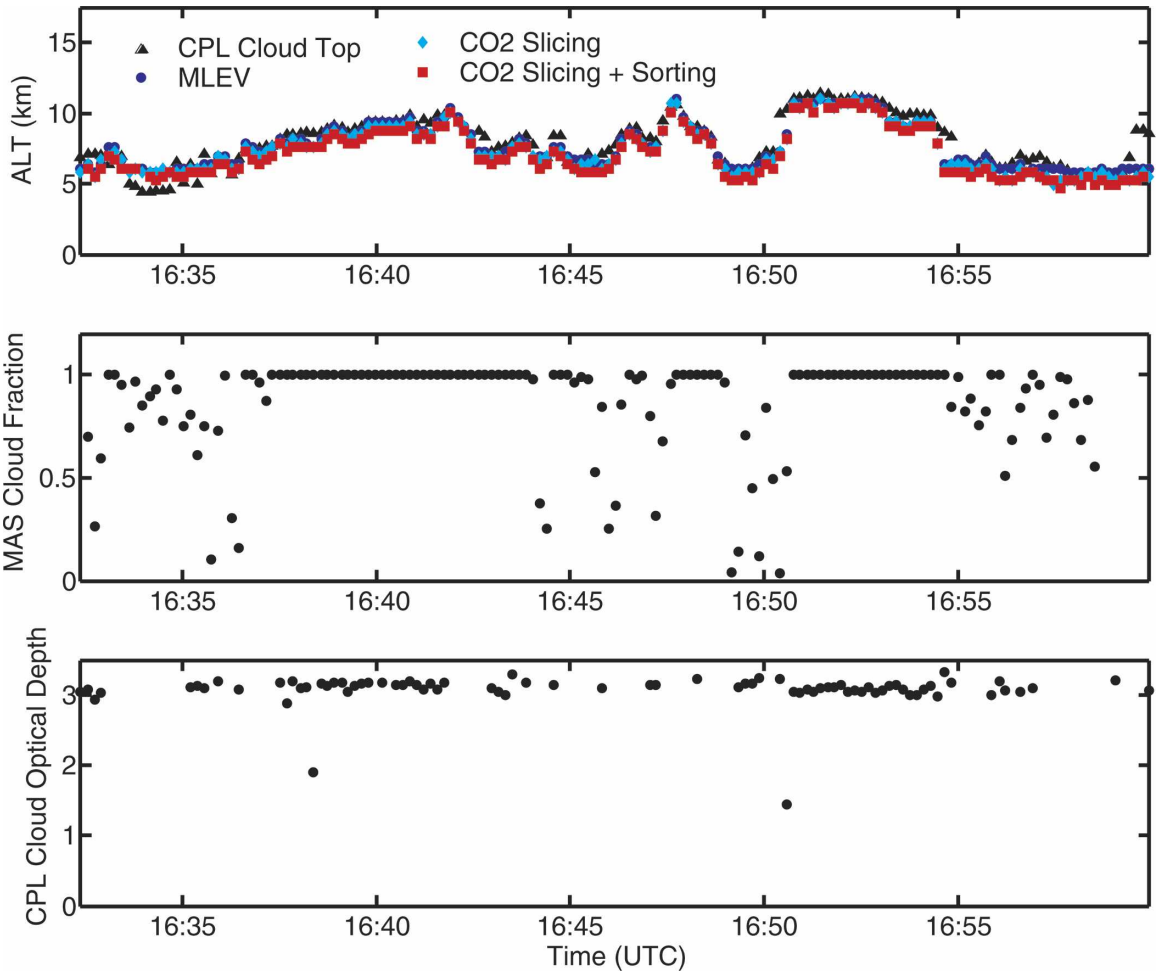

FIG. 10. (top) The S-HIS cloud-top retrievals collocated with the CPL-measured cloud-top and -base measurements from 5 Dec 2003. (middle) The cloud fraction is computed using the collocated MAS pixels for each S-HIS field of view. The MAS cloud mask is applied to the collocated MAS pixels and the cloud fraction is computed from the cloud mask results. (bottom) The mean CPL-measured optical depth is presented. The cloud top, base, and optical depth are the mean of all of the CPL measurements found to be in each S-HIS field of view.

12–13 km were detected by the CPL (Fig. 5). The CPL cloud extinction profile in Fig. 5 shows that the cloud extinction increases toward the lower levels of the cloud. The CPL-measured depolarization remains above 25%, except near 0140 UTC where the cloud depolarization is as low as 20%. For our purposes, CPL measurements of clouds with depolarization of greater than 25% are ice while depolarization of less than 10% are generally water clouds. It would be unusual to have liquid water above 10 km. A possible explanation for the low depolarization at this level is a change in ice habit, perhaps from small droxtals nearly spherical in shape, because the amount of depolarization is dependent on the ice crystal shape.

Figure 6 presents the S-HIS cloud-top retrievals with the collocated CPL cloud boundaries. The CPL has a maximum optical depth sensitivity of approximately 3.2 (McGill et al. 2004). For this reason, when interpreting the CPL cloud boundaries, the actual cloud geometrical thickness may be larger than that presented in Fig. 6 if the actual cloud optical depth is greater than 3.2. If the CPL does not detect a lower cloud or ground return, the CPL-retrieved cloud base is not presented. The S-HIS cloud fraction in Fig. 6 is retrieved by applying the MAS cloud mask algorithm to the collocated MAS pixels within each S-HIS FOV.

The region between 1315 and 1330 UTC shows the largest variations compared to the CPL cloud height. During this period the CPL optical depth measurements ranged between 0.5 and 2.5. The largest differences were found when the cloud fraction is less than 1.0 at approximately 1327 UTC. This cloud presents a

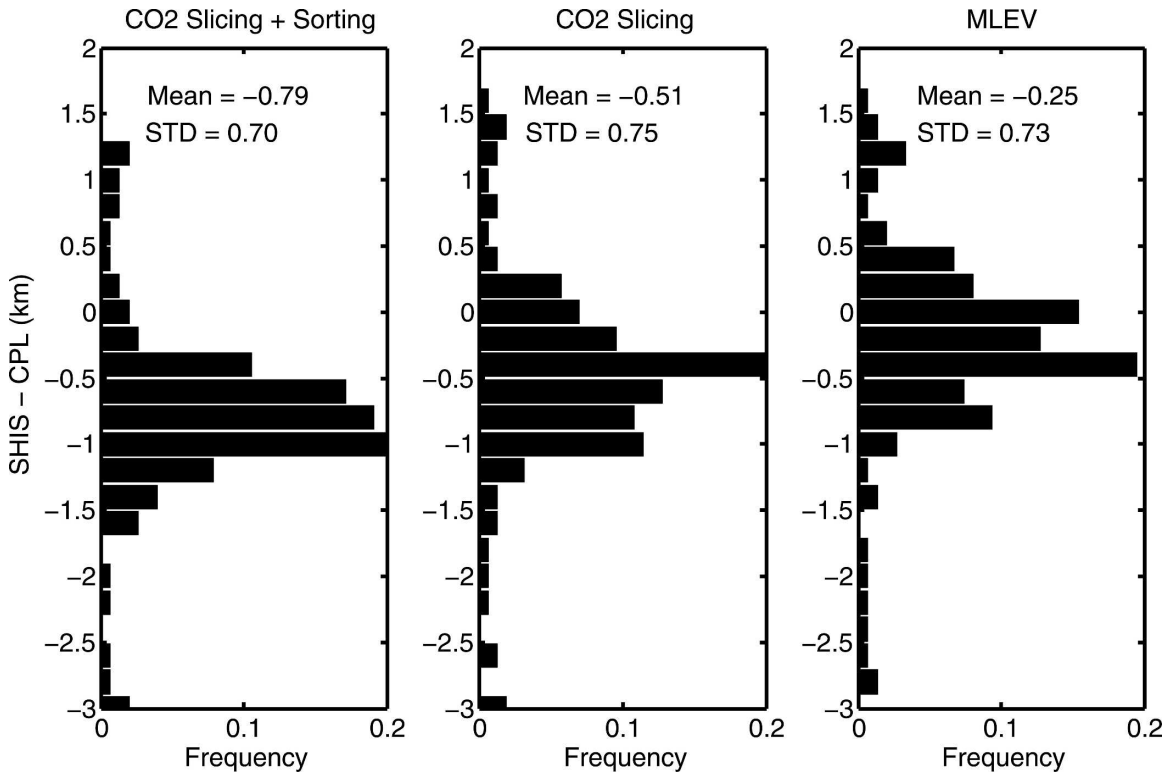

FIG. 11. The frequency of occurrence of the differences between the S-HIS cloud-top retrieval height compared to the mean of the collocated CPL cloud height is presented for the different S-HIS retrievals for the flight on 5 Dec 2003.

challenging environment for the S-HIS cloud-top altitude retrievals. For this period, the CO_2 hybrid slicing–sorting algorithm results demonstrate the closest agreement to the CPL cloud height. The fixed CO_2-slicing and MLEV retrievals significantly underestimate the cloud top. The largest differences between the CPL and S-HIS cloud heights occur at 1327 UTC when the S-HIS FOV is partially cloud filled as determined by the MAS cloud fraction.

After 1330 UTC the cloud optical depth remains greater than 3.0 for most of the profile as determined by the CPL. Between 1330 and 1335 UTC there is better agreement between the S-HIS- and CPL-retrieved cloud-top altitude. After 1335 UTC the S-HIS and CPL cloud-top altitude diverge with the S-HIS retrievals underestimating the cloud-top altitude. By 1345 UTC the S-HIS-retrieved cloud top differs by as much as 2.5 km compared to that of the CPL. Despite the large differences between the CPL and the infrared retrievals, the three infrared cloud-top retrievals compare closely.

The distribution of the differences between the collocated CPL-measured cloud-top height compared to the S-HIS cloud-top height retrieval is presented in Fig. 7. The differences between the CPL and S-HIS are calculated using the mean cloud-top height of the CPL measurements found for each S-HIS FOV. A negative difference results if the S-HIS retrieval is lower than the CPL-retrieved cloud height. Figure 7 confirms that there is significant variability between the CPL and S-HIS cloud-top altitude retrievals. The fixed-channel CO_2 slicing, hybrid CO_2 slicing–sorting, and MLEV compare closely with mean differences of -1.45, -1.52, and -1.39 km, respectively. The width of distributions differs with the hybrid CO_2 slicing–sorting having a narrower distribution of ± 0.70 km compared to fixed-channel CO_2 slicing and MLEV with standard deviations of ± 1.30 and 2.0 km.

The differences in the sensitivities between the three algorithms become apparent when only S-HIS FOVs with collocated CPL total cloud optical thickness less than 1.0 are considered, as presented in Fig. 8. For optically thin clouds the hybrid CO_2 slicing–sorting retrieval significantly reduces the cloud-height biases. MLEV overestimates the cloud height for these optically thin FOV as presented in Fig. 6.

b. ATReC Atlantic

The ER-2 flew during the ATReC field experiment based in Bangor in the fall of 2003 as part of the Global Atmospheric Research Program (GARP). In addition

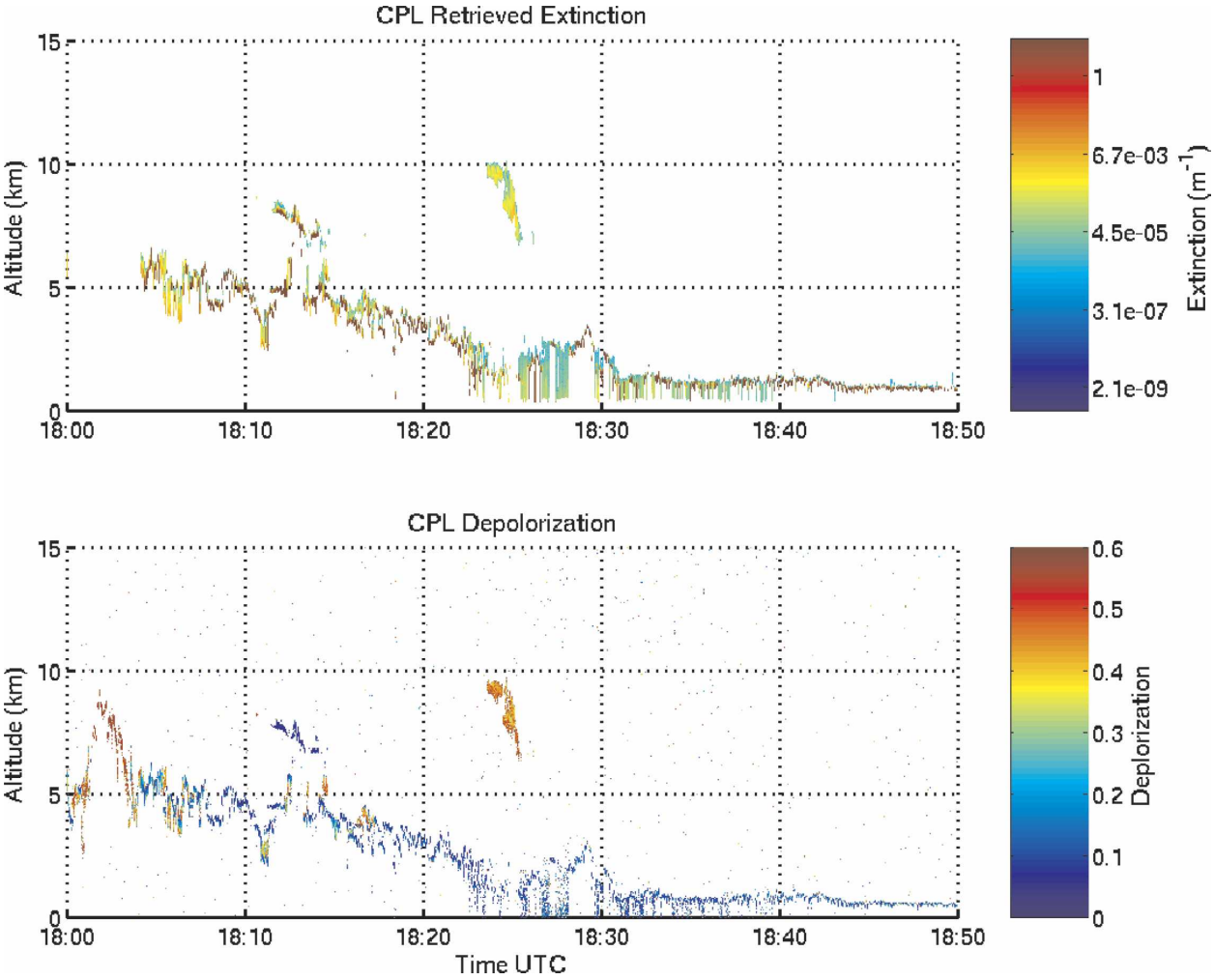

FIG. 12. The CPL-retrieved extinction and depolarization from the Atlantic THORPEX experiment on 5 Dec 2003.

to the MAS, CPL, and S-HIS on the ER-2, the University of North Dakota Citation aircraft flew during the experiment with an extensive array of in situ measurements that included dropsondes. This paper will focus on the 5 December 2003 ER-2 flight that over flew a variety of cloud types ranging from high cirrus to stratus.

1) ER2 FLIGHT TRACK: 1630–1700 UTC

The ER-2 flight segment between 1630 and 1700 UTC is characterized by diverse cloud conditions. The CPL-measured cloud-top and depolarization indicate rapidly changing cloud height and phase as presented in Fig. 9. The CPL-measured cloud depolarization varies between 2.0% and 50%, signifying a mixed-phase environment.

The S-HIS cloud-top altitude retrievals collocated with the CPL- and MAS-retrieved cloud properties are presented in Fig. 10. The S-HIS cloud-top retrievals follow well with the CPL cloud-top heights during this flight segment. The beginning of the flight segment (1630–1637 UTC) demonstrates the greatest variability between the S-HIS and CPL cloud-top retrievals, with all three retrievals overestimating the cloud height. Broken and multilevel clouds characterize this time period as determined by the collocated CPL and MAS measurements. Between 1637 and 1650 UTC all of the S-HIS cloud-top retrievals detect the cloud with good agreement with the CPL.

The peak of the hybrid CO_2 slicing–sorting difference distribution presented in Fig. 11 compares closely with the CPL cloud heights, with mean differences less than 1.0 km for all three retrievals. The tendency for the cloud-top retrievals to overestimate the cloud height when the S-HIS FOV is partially cloud filled is apparent in Fig. 11 as the small peak with positive dif-

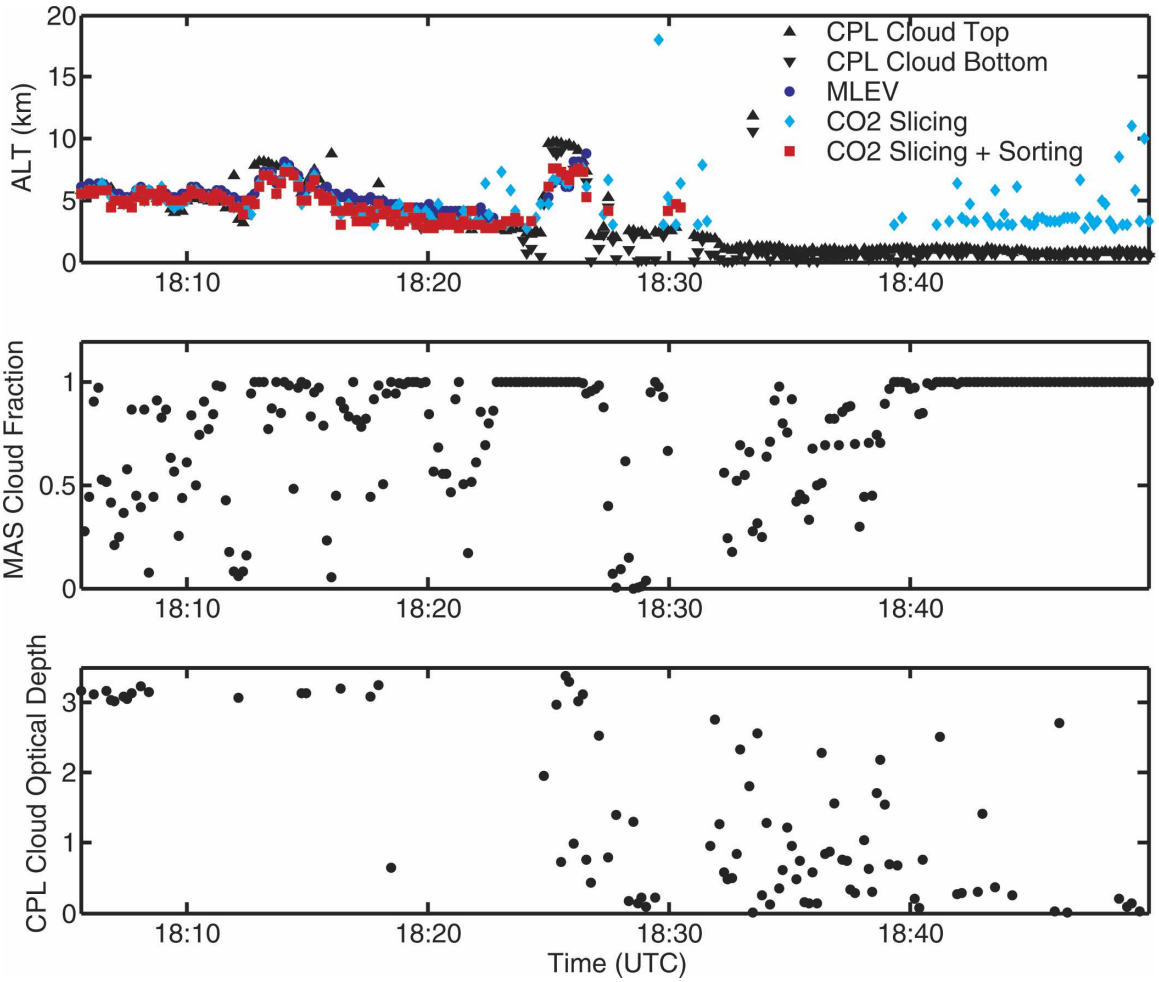

FIG. 13. (top) The S-HIS cloud-top retrievals collocated with the CPL-measured cloud-top and -base measurements from 5 Dec 2003. (middle) The MAS cloud fraction and (bottom) the mean CPL-measured optical depth are presented. The cloud top, base, and optical depth are the mean of all the CPL measurements found to be in each S-HIS field of view.

ferences (S-HIS-retrieved cloud height is above the CPL).

2) ER-2 FLIGHT TRACK: 1800–1850 UTC

The beginning of the flight segment (1805–1830 UTC) contains broken midlevel clouds with a thin cirrus layer over low stratus existing between 1826 and 1828 UTC, as presented in Fig. 12. The hybrid CO_2 slicing–sorting, fixed-channel pair CO_2-slicing, and MLEV retrievals detect the midlevel cloud but have considerable variability compared to the CPL cloud height, as presented in Fig. 13.

The flight segment after 1830 UTC consists of low marine broken cumulous that progressively becomes overcast based on the MAS-derived cloud fraction in Fig. 13. Between 1833 and 1839 UTC the hybrid CO_2 slicing and MLEV do not detect the broken cumulous while the fixed-channel CO_2 slicing detects the cumulus when the S-HIS cloud fraction is greater then 70%. When the fixed-channel CO_2 does retrieve the cloud height, it overestimates the cloud top. The distribution of difference between the collocated S-HIS and CPL cloud heights is presented in Fig. 14.

5. Discussion

This paper has presented a comparison of infrared hyperspectral cloud-top altitude retrieval algorithms, including CO_2 sorting–slicing, a new method to select optimal channel pairs for CO_2 slicing. The following discussion will interpret the results using the collocated MAS and CPL measurements with a focus on the periods when there was disagreement between the S-HIS and CPL cloud-top altitude retrievals.

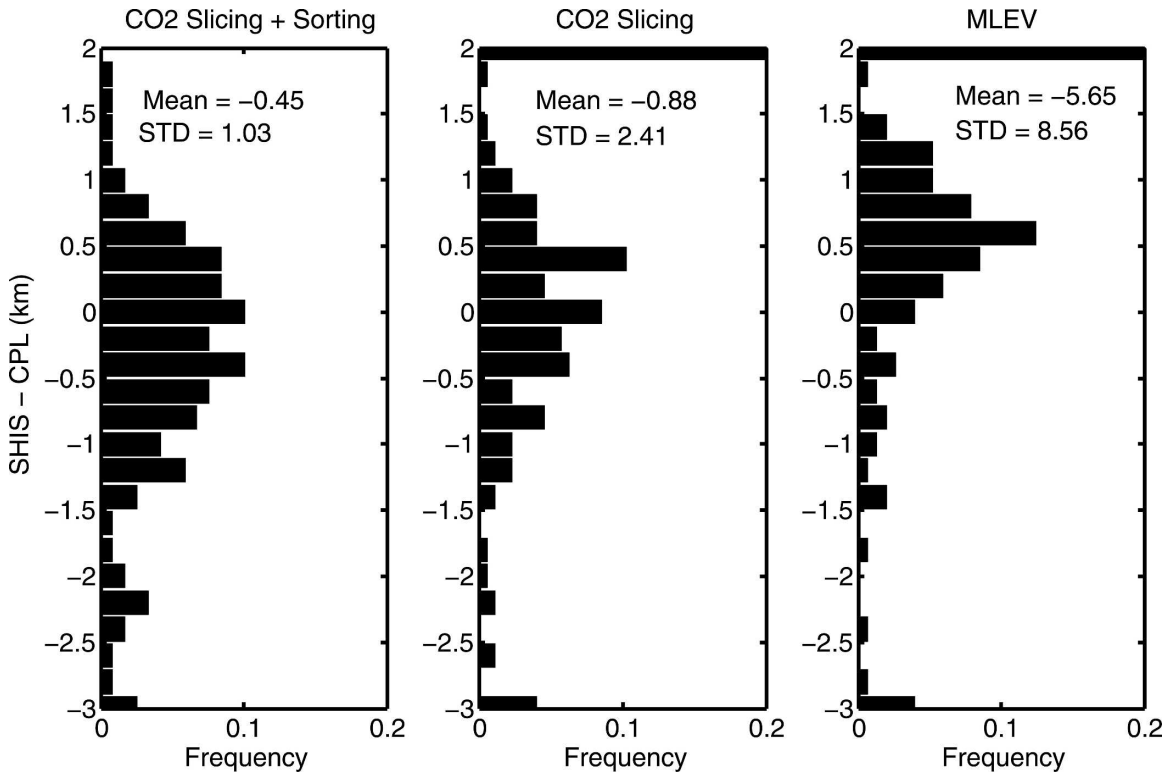

FIG. 14. The frequency of occurrence of the differences between the S-HIS cloud-top retrieval height compared to the mean of the collocated CPL cloud height is presented for the different S-HIS retrievals for the flight on 5 Dec 2003.

For the cases presented, when combined with CO_2 slicing, the sorting significantly improves the cloud-top altitude retrieval for optically thin clouds compared to the fixed-channel pair CO_2 slicing alone. For optically thin clouds the difference between the measured cloudy radiance $I(\upsilon)$ and the clear-sky-simulated radiance $I_{cl}(\upsilon)$ in the CO_2-slicing equation [Eq. (1)] becomes small with measured minus clear differences less than 2 (MW str^{-1} μm^{-1}). For this reason CO_2 slicing is sensitive to the accuracy of the clear-sky radiance calculation, which is dependent on a priori knowledge of the lower-atmospheric temperature, water vapor, and surface temperature and emissivity. The hybrid CO_2 slicing–sorting method reduces the cloud retrieval biases for thin clouds by selecting channel pairs that maximize the sensitivity to the cloud level but not the surface. Reducing the surface contribution reduces the retrieval sensitivity to errors in the lower-atmospheric state. The hybrid CO_2 slicing–sorting algorithm reduces the large 4–5-km cloud-height differences observed using fixed-channel CO_2 slicing and MLEV based on a comparison with the collocated CPL cloud heights for thin clouds (optical depths less than 1.0), as highlighted in Fig. 8. This improvement is reflected in the reduced standard deviation of the hybrid CO_2 slicing compared to MLEV and fixed-channel pair CO_2 slicing.

Large differences (greater than 3 km) in cloud-top altitude retrievals between the S-HIS and the CPL occurred in Fig. 6 between 01:25 and 01:55 UTC. The cloud as detected by the CPL cloud extinction in Fig. 5 is geometrically thick but optically tenuous cirrus. This case represents a condition where the different sensitivities between the CPL and S-HIS can result in large differences in the retrieved cloud-top height. The CPL measures the backscattered intensity while the S-HIS measures primarily atmospheric emission. The intensity of the backscatter measured by the CPL is a function of the cloud backscatter cross section while the S-HIS cloud signal is dependent on the cloud optical depth. Cirrus microphysical properties can result in a significant lidar return well above the level at which the integrated cloud optical depth becomes large enough to be detected by the S-HIS retrievals.

To investigate the differences found in Fig. 6, collocated CPL extinction profiles are integrated starting from the top of the cloud to produce integrated optical depth contours at each CPL level in the cloud. Using the integrated CPL extinction, the integrated optical depth at the level the S-HIS retrieval detected the cloud is determined as illustrated in Fig. 15.

The geometric S-HIS–CPL cloud-height differences and integrated optical depths using the method de-

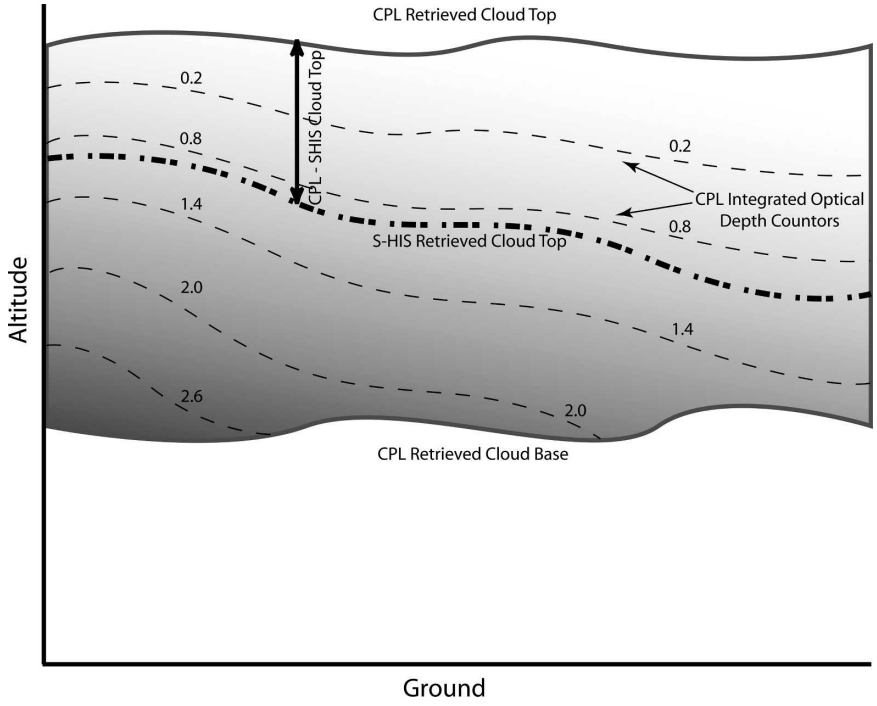

FIG. 15. A cartoon to demonstrate the method used to determine the CPL-integrated cloud optical depth at the level of the S-HIS retrieval. The optical depth contours are determined by integrating the CPL extinction profile through the cloud.

scribed in Fig. 15 for the 22 February flight between 01:30 and 01:50 UTC are presented in Fig. 16 and Fig. 17. The S-HIS–CPL cloud-height differences progress from relatively close agreement at 1330 UTC to differences of larger than 2.5 km at 1345 UTC. Despite the large geometric differences, the integrated optical depth at the level that the S-HIS detected the cloud height remains relatively constant with a mean optical depth of approximately 1.0. The distribution of integrated CPL optical depths at the level of the S-HIS-retrieved cloud height in Fig. 17 shows a sharp peak at optical depth 1.0.

This result illustrates the importance of considering instrument sensitivities to cloud microphysical characteristics when comparing cloud-height results. It raises the following question: what is the correct cloud-top height when two independent measurements can accurately measure the cloud height but differ by more than 2.5 km? The answer depends on the application. For infrared cloud radiative processes the S-HIS cloud-top-retrieved altitude may be a more representative measurement, while the lidar cloud top is best applied to visible cloud characteristics. When lidar measurements are used to validate infrared cloud-top altitude retrievals, this result suggests that the lidar-retrieved integrated extinction is a more representative measurement when comparing to infrared cloud-top retrievals.

Low clouds (below 3.0 km) present a challenging environment for IR cloud retrievals. The largest uncertainties in the temperature and water vapor profiles are in the lower atmosphere, and the difference between the cloud and surface temperatures are small, reducing the cloudy minus clear-sky difference in Eq. (1). As expected, large differences between the S-HIS cloud-top retrievals and the CPL were found for low clouds.

The ability of the CO_2 sorting to detect low clouds depends on the clear-sky FOV. For this investigation the clearest FOV for the flight track was selected by using the FOV with the warmest window brightness temperature. A cloud-contaminated clear-sky FOV will degrade the already weak contrast between low clouds and the sorted clear scene, reducing the reliability of the sorting algorithm channel selection. Additionally, the hybrid CO_2 slicing purposefully rejects channels that have significant surface sensitivity. If the cloud is very near the surface, the hybrid algorithm will pick channels that peak above the cloud, further reducing the sensitivity. Future work will address this issue by using selected channel pairs that are optimized for low clouds when CO_2 sorting determines low clouds in the FOV. An alternative would be to use a water vapor–corrected brightness temperature retrieval.

The fixed-channel pair CO_2 slicing uses fixed mi-

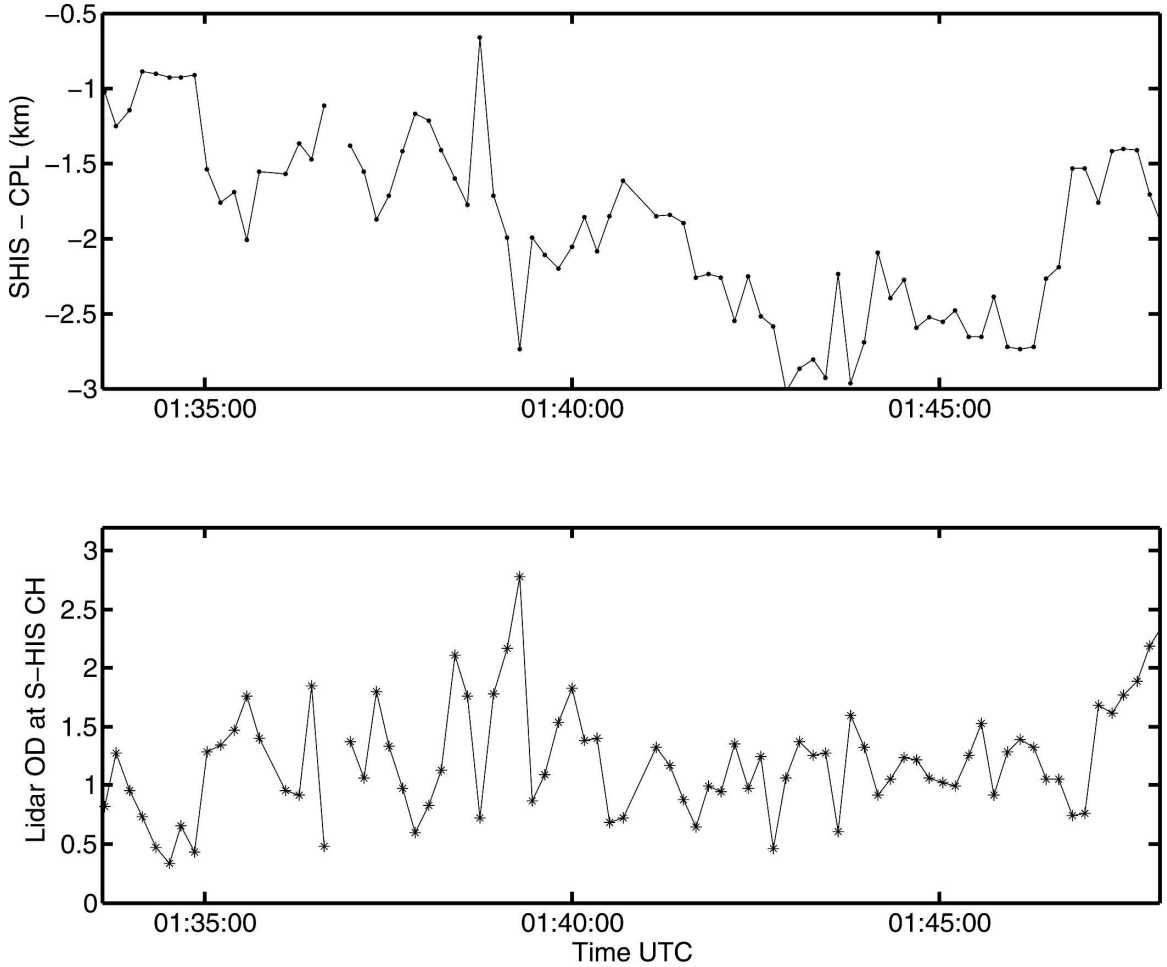

FIG. 16. The geometric difference between the S-HIS hybrid slicing–sorting retrieval and the collocated CPL cloud height for the 22 February flight is presented in this figure. The integrated optical depth determined by the CPL at the level of the S-HIS hybrid retrieved cloud height (CH) is presented in the lower plot. Notice that integrated optical depth remains relatively constant while the S-HIS–CPL cloud height differences vary between 0.5 and 3.0 km.

crowindow channels in the CO_2 band (740–800 cm^{-1}). The relatively transparent microwindows have weighting functions that peak near the surface. For low clouds these channels should optimize the CO_2-slicing retrieval, possibly explaining the increased sensitivity for low clouds. The MLEV retrieval's lack of sensitivity to low clouds supports the findings of Huang et al. (2004).

The ability to detect and retrieve cloud heights is dependent on the accuracy of the clear-sky temperature and water vapor profile used to simulate the clear-sky radiances used in the retrieval. For this investigation well-characterized atmospheric profile information was available using S-HIS temperature and water vapor retrievals and aircraft dropsondes. For satellite retrievals global temperature and water vapor profiles are required. The accuracy of the atmospheric profile measurements will impact the sensitivity and accuracy of the retrievals, especially for optically thin or low clouds. The hybrid CO_2 slicing–sorting retrieval has the potential to reduce cloud-height errors caused by atmospheric profile uncertainties by selecting channels that are sensitive to the cloud level but insensitive to the lower atmosphere where large uncertainties in lower-atmospheric temperature, water vapor, and surface characteristics exist.

6. Summary

This paper presents a new algorithm that optimizes the high-spectral-resolution CO_2-slicing cloud-top retrievals. The capabilities of the optimized hyperspectral CO_2-slicing retrieval is demonstrated using observations from the S-HIS during the THORPEX and ATReC experiments. The analysis includes a compari-

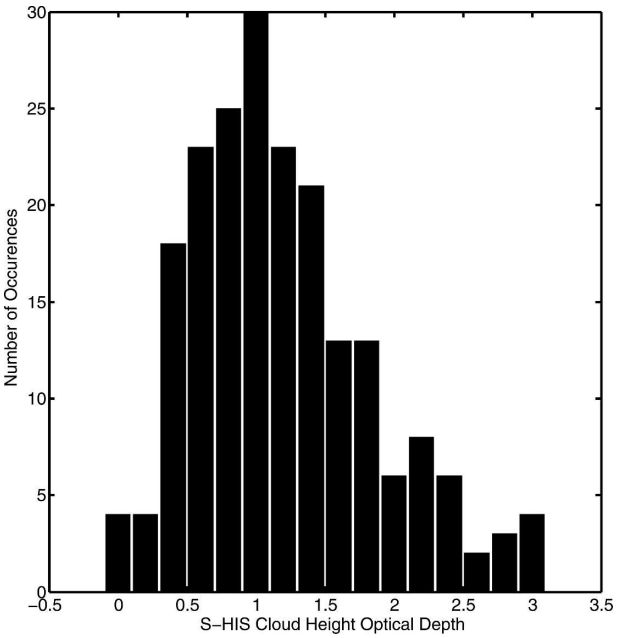

FIG. 17. The frequency of occurrence of the CPL-integrated optical depth at the level of the S-HIS CO_2-sorting–slicing hybrid-retrieved cloud height from the 22 February ER-2 flight between 1307 and 1400 UTC is presented in this figure. Notice that the optical depths peak between 0 and 1.0.

son with the CPL measurements, an active sensor used to retrieve the cloud-top altitude and cloud optical depth. MAS measurements are collocated with the S-HIS FOVs to determine the fractional cloud coverage in the S-HIS FOV. From these comparisons the sensitivity of the passive IR algorithms to cloud height, optical depth, and cloud fraction is investigated using the collocated lidar (CPL) and imager (MAS) measurements. It is found that the agreement between the CPL and S-HIS infrared retrievals is strongly dependent on the cloud radiative characteristics, and for optically thin clouds the hybrid CO_2 sorting–slicing algorithm reduced the frequency of large biases when compared to the fixed-channel CO_2 slicing and MLEV.

For geometrically thick but optically tenuous cirrus clouds the infrared cloud-top retrievals significantly underestimated the cloud height by greater than 2.5 km when compared to the CPL. For these cases the S-HIS cloud-top retrievals were compared to the CPL-integrated optical depth normalized to the CPL-retrieved cloud top. It is found that for these cases the infrared cloud-top retrieval correlates closely to the level in the cloud where the CPL-integrated optical depth is approximately 1.0. This result has important implications for satellite cloud-height validation. Global lidar measurements of cloud heights are currently available using Geoscience Laser Altimeter System (GLAS) (Zwally et al. 2002) data and will soon be available with the launch of Cloud-Aerosol Lidar and Infrared Pathfinder Satellite Observations (CALIPSO) (Winker and Wielicki 2000). The measurements offer a validation dataset to compare to infrared cloud retrievals such as MODIS and AIRS. This investigation suggests that for geometrically thick but optically thin cirrus large differences between the lidar and passive IR remotely sensed cloud-top heights should be expected and that these differences result from differences in instrument sensitivities, not retrieval errors.

Future research plans include applications to additional aircraft measurements and continued development of the CO_2 slicing–sorting retrieval to improve the sensitivity of the algorithm to low clouds. Implementation of the CO_2 sorting–slicing retrieval to satellite-based hyperspecteral measurements (AIRS) are planned.

Acknowledgments. The authors would like to gratefully thank the S-HIS research team for supplying the S-HIS measurements used in this paper. We would like to acknowledge Ray Garcia for his help with understanding the S-HIS data processing. We thank the MAS instrument and cloud mask research groups for supplying the MAS measurements and cloud mask. The NASA Goddard Suomi–Simpson fellowship program funded this research.

REFERENCES

Ackerman, S. A., K. I. Stabala, W. P. Menzel, R. A. Frey, C. Moeller, and L. E. Gumley, 1998: Discriminating clear sky from clouds with MODIS. *J. Geophys. Res.,* **103,** 32 141–32 157.

Aumann, H. H., and Coauthors, 2003: AIRS/AMSU/HSB on the Aqua mission: Design, science objectives, data products, and processing systems. *IEEE Trans. Geosci. Remote Sens.,* **41,** 253–264.

Chahine, M. T., 1974: Remote sounding of cloudy atmospheres. I. The single cloud layer. *J. Atmos. Sci.,* **31,** 233–243.

Clough, S. A., F. X. Kneizys, L. S. Rothman, and W. O. Gallery, 1981: Atmospheric Spectral Transmittance and Radiance—Fascod1b. *Proc. Soc. Photo-Opt. Instrum. Eng.,* **277,** 152–166.

Hawkinson, J. A., W. Fleltz, and S. A. Ackerman, 2005: A comparison of GOES sounder and cloud lidar- and radar-retrieved cloud-top heights. *J. Appl. Meteor.,* **44,** 1234–1242.

Huang, H. L., W. L. Smith, L. Li, P. Antonelli, X. Wu, R. O. Knuteson, B. Huang, and B. J. Osborne, 2004: Minimum local emissivity variance retrieval of cloud altitude and effective spectral emissivity—Simulation and initial verification. *J. Appl. Meteor.,* **43,** 795–809.

King, M. D., and Coauthors, 1996: Airborne scanning spectrometer for remote sensing of cloud, aerosol, water vapor, and surface properties. *J. Atmos. Oceanic Technol.,* **13,** 777–794.

McGill, M., D. Hlavka, W. Hart, V. S. Scott, J. D. Spinhirne, and B. Schmid, 2002: Cloud Physics Lidar: Instrument description and initial measurement results. *Appl. Opt.,* **41,** 3725–3734.

McGill, M. J., and Coauthors, 2004: Combined lidar-radar remote sensing: Initial results from CRYSTAL-FACE. *J. Geophys. Res.,* **109,** D07203, doi:10.1029/2003JD004030.

McNally, A. P., and P. D. Watts, 2003: A cloud detection algorithm for high-spectral-resolution infrared sounders. *Quart. J. Roy. Meteor. Soc.,* **129,** 3411–3423.

Menzel, W. P., L. W. Smith, and T. R. Stewart, 1983: Improved cloud motion wind vector and altitude assignment using VAS. *J. Climate Appl. Meteor.,* **22,** 377–384.

Nagel, F. W., 1998: The association of disparate satellite observations. Preprints, *Second Symp. of Integrated Observing Systems*, Phoenix, AZ, Amer. Meteor. Soc., 49–52.

Ohring, G., B. Wielicki, R. Spencer, B. Emery, and R. Datla, 2005: Satellite instrument calibration for measuring global climate change: Report of a workshop. *Bull. Amer. Meteor. Soc.,* **86,** 1303–1313.

Revercomb, H. E., and Coauthors, 1998: Recent results from two new aircraft-based fourier-transform interferometers: The Scanning High-resolution Interferometer Sounder and the NPOESS Atmospheric Sounder Testbed Interferometer. *Eighth Int. Workshop on Atmospheric Science from Space Using Fourier Transform Spectrometry*, Toulouse, France, 1–6.

Shapiro, M. A., and A. J. Thorpe, 2002: Report on the current status of the observing-system research and predictability experiment (THORpex). *First Int. THORpex Workshop,* Potomac, MD.

Smith, W. L., 1970: A regression method for obtaining real-time temperature and geopotential height profiles from satellite spectrometer measurements and its application to Nimbu-3 SIRS observations. *Mon. Wea. Rev.,* **98,** 604–611.

——, and C. M. R. Platt, 1978: Comparison of satellite-deduced cloud heights with indications from radiosonde and ground-based laser measurements. *J. Appl. Meteor.,* **17,** 1796–1802.

——, and R. Frey, 1990: On cloud altitude determinations from High-Resolution Interferometer Sounder (HIS) observations. *J. Appl. Meteor.,* **29,** 658–662.

——, H. M. Wolf, P. G. Abel, C. M. Hayden, M. Chalfant, and N. Grody, 1974: Nimbus 5 sounder data processing system. Part I: Measurement characteristics and data reduction procedures. NOAA Tech. Memo. NESS 57, National Oceanic and Atmospheric Administration, 99 pp.

Winker, D. M., and B. Wielicki, 2000: PICASSO-CENA mission. *Conf. on Sensors, Systems, and Next-Generation Satellites VI,* Barcelona, Spain, SPIE, 26–36.

Wylie, D. P., and W. P. Menzel, 1989: Two years of cloud cover statistics using VAS. *J. Climate,* **2,** 380–392.

Zwally, H. J., and Coauthors, 2002: ICESat's laser measurements of polar ice, atmosphere, ocean, and land. *J. Geodyn.,* **34,** 405–445.